REFERENCES AND NOTES

1. G. B. Lubkin, *Phys. Today* **49**, 48 (March 1996); D. C. Larbalestier and M. P. Maley, *Mater. Res. Soc. Bull.* **18**, 50 (1993).
2. P. M. Grant, *Nature* **375**, 107 (1995).
3. A. E. Pashitski, A. Polyanskii, A. Gurevich, J. A. Parrell, D. C. Larbalestier, *Physica C* **246**, 133 (1995).
4. D. J. Bishop, P. L. Gammel, D. A. Huse, C. A. Murray, *Science* **255**, 165 (1992).
5. D. S. Fisher, M. P. A. Fisher, D. A. Huse, *Phys. Rev. B* **43**, 130 (1991).
6. G. Blatter, M. V. Feigel'man, V. B. Geshkenbein, A. I. Larkin, V. M. Vinokur, *Rev. Mod. Phys.* **66**, 1125 (1994).
7. A. P. Malozemoff, in *Physical Properties of High Temperature Superconductors*, D. Ginsberg, Ed. (World Scientific, Singapore, 1989), pp. 71–150.
8. U. Welp *et al.*, *Nature* **376**, 44 (1995).
9. W. L. Carter *et al.*, *IEEE Trans. Appl. Supercond.* **5**, 1145 (1995); C. J. Christopherson and G. N. Riley Jr., *Appl. Phys. Lett.* **66**, 2277 (1995); K. Sato *et al.*, *Physica B* **216**, 258 (1996); K. Ohkura, K. Sato, M. Ueyama, J. Fujikami, Y. Iwasa, *Appl. Phys. Lett.* **67**, 1923 (1995).
10. D. C. Larbalestier *et al.*, *Physica C* **221**, 299 (1994); M. Lelovic, P. Krishnaraj, N. G. Eror, U. Balachandran, *ibid.* **242**, 246 (1995).
11. Q. Li, H. J. Wiesmann, M. Suenaga, L. Motowidlo, P. Haldar, *Appl. Phys. Lett.* **66**, 637 (1995).
12. P. Majewski, *Adv. Mater.* **6**, 593 (1994).
13. The problem of thermally activated flux motion is less severe in the HTSC YBa$_2$Cu$_3$O$_7$ (YBCO) and hence it offers better intrinsic behavior at high temperatures and magnetic fields. The processing strategies developed for BSCCO fail to yield viable YBCO wires as a result of poor intergranular current flow. Recent work suggests, however, that good alignment between grains can be achieved in thick films deposited on nickel tapes by ion beam deposition [X. D. Wu *et al.*, *Appl. Phys. Lett.* **67**, 2397 (1995)]. The commercial viability of this strategy remains to be demonstrated.
14. D. R. Nelson and V. M. Vinokur, *Phys. Rev. Lett.* **68**, 2398 (1992); ______, *Phys. Rev. B* **48**, 13060 (1993).
15. T. Hwa, P. Le Doussal, D. R. Nelson, V. M. Vinokur, *Phys. Rev. Lett.* **71**, 3545 (1993).
16. L. Civale *et al.*, *ibid.* **67**, 648 (1991); M. Konczykowski *et al.*, *Phys. Rev. B* **44**, 7167 (1991); R. C. Budhani, M. Suenaga, S. H. Liou, *Phys. Rev. Lett.* **69**, 3816 (1992); W. Gerhauser *et al.*, *ibid.*, **68**, 879 (1992); J. R. Thompson *et al.*, *Appl. Phys. Lett.* **60**, 2306 (1992); L. Civale *et al.*, *Physica C* **208**, 137 (1993).
17. P. Kummeth *et al.*, *J. Alloys Compd.* **195**, 403 (1993); P. Kummeth, C. Struller, H.-W. Neumuller, G. Saemann-Ischenko, *Appl. Phys. Lett.* **65**, 1302 (1994).
18. H. Dai, S. Yoon, J. Liu, R. C. Budhani, C. M. Lieber, *Science* **265**, 1552 (1994); U. C. Tauber, H. Dai, D. R. Nelson, C. M. Lieber, *Phys. Rev. Lett.* **74**, 5132 (1995).
19. Y. Zhu, Z. X. Cai, R. C. Budhani, M. Suenaga, D. O. Welch, *Phys. Rev. B* **48**, 6436 (1993).
20. J. R. Thompson, D. Paul, Z. L. Wang, D. M. Kroeger, D. K. Christen, *Appl. Phys. Lett.* **67**, 1007 (1995).
21. L. Krusin-Elbaum *et al.*, *ibid.* **64**, 3331 (1994).
22. H. Safar *et al.*, *ibid.* **67**, 130 (1995).
23. P. Le Doussal and D. R. Nelson, *Physica C* **232**, 69 (1994).
24. K. Fossheim, E. D. Tuset, T. W. Ebbesen, M. M. J. Treacy, J. Schwartz, *ibid.* **248**, 195 (1995).
25. A recent report of carbon nanotube-BSCCO composites (*24*) showed some evidence of J_c improvement; however, the J_c value of both the reference and nanorod-containing sample in this report were lower than the good-quality BSCCO samples reported previously and in the present study. It is thus difficult to conclude that there is an improvement in behavior upon adding nanotubes. In addition, this report and our own studies show that few nanotubes survive the synthesis process, leaving in doubt their ability to create well-defined columnar defects in the HTSCs.
26. N. Adamopoulos, B. Soylu, Y. Yan, J. E. Evetts, *Physica C* **242**, 68 (1995).
27. Y. S. Yuan, M. S. Wong, S. S. Wang, *J. Mater. Res.* **11**, 8 (1996); *Physica C* **250**, 247 (1995).
28. H. Dai, E. W. Wong, Y. Z. Lu, S. Fan, C. M. Lieber, *Nature* **375**, 769 (1995).
29. P. Yang and C. M. Lieber, in preparation.
30. H. Itoh, S. Utamapanya, J. V. Stark, K. J. Klabunde, J. R. Schlup, *Chem. Mater.* **5**, 71 (1993).
31. K. Sangwal, *J. Mater. Sci.* **17**, 3598 (1982).
32. Nanorod-HTSC composites have also been successfully prepared with TlBa$_2$Ca$_2$Cu$_3$O$_9$ and Tl$_2$Ba$_2$Ca$_2$Cu$_3$O$_{10}$ materials. Preliminary measurements show that there are significant enhancements in J_c for these composites (P. Yang and C. M. Lieber, unpublished results).
33. C. Li, S. Patel, J. Ye, E. Narumi, D. T. Shaw, *Appl. Phys. Lett.* **63**, 2558 (1993).
34. The actual density of columnar defects that can pin flux lines may be larger than that corresponding to the density of MgO nanorods; that is, lattice strains associated with nanorod-BSCCO interfaces can lead to dislocations and other correlated defects that exhibit columnarlike pinning behavior.
35. The density of nanorods oriented close to the *c* axis was about 1×10^{10} cm^{-2}; a similar density was determined for nanorods oriented in the *ab* plane. Although this density is significantly lower than that obtained by heavy-ion and proton irradiation, we have not tried to maximize the density of MgO nanorods and also believe that the density of correlated defects is probably significantly higher than that of nanorods (*34*).
36. C. P. Bean, *Rev. Mod. Phys.* **36**, 31 (1964).
37. An inverse dependence of J_c on defect size was also reported previously for Y$_2$BaCuO$_5$ inclusions of 1 to 10 μm in diameter in YBCO [M. Murakami, in *Phenomenology and Applications of High-Temperature Superconductors*, K. S. Bedell, M. Inui, D. Meltzer, J. R. Schrieffer, S. Doniach, Eds. (Addison-Wesley, New York, 1992), p. 103].
38. A. Morales, P. Yang, C. M. Lieber, *J. Am. Chem. Soc.* **116**, 8360 (1994).
39. The MgO nanorods were grown as follows: a mixture of MgO (Alfa, 1 μm) and graphite powder (Alfa, 300 mesh), 1:3 to 3:1 weight ratio, was ground and placed in a graphite boat inside a quartz furnace tube. MgO nanoclusters 5 to 8 nm in diameter (*30*) or a MgO (100) single crystal, which had been etched with a NiCl$_2$ solution (*31*), was placed in a second graphite boat, and the tube was purged with Ar; the nucleation sites were located downstream of the MgO-carbon mixture. With the Ar flowing, the quartz tube was heated at a temperature of 1200°C for 0.5 to 2 hours and then cooled to room temperature. MgO nanorods were isolated from the graphite boat containing the MgO nanocluster or etched (100) MgO surface.
40. The amorphous BSCCO film was deposited at room temperature by laser ablation of a Bi$_{2.2}$Sr$_2$CaCu$_2$O$_x$ target in 200 mtorr of oxygen with a pulse energy of 1 J cm^{-2} (*38*). Bulk composites were made by (i) mixing BSCCO-2212 powder with MgO nanorods (~15% weight ratio), (ii) pressing the mixture into a pellet, and (iii) melt-texturing the resulting pellet on silver foil. The texturing procedure used to prepare both types consisted of partial melting at 860° to 880°C and then cooling to 780°C at a rate of 1° to 5°C hour^{-1}; after annealing at 780°C for 10 to 24 hours, samples were cooled to room temperature. The T_c's of composite and reference samples prepared in this way were typically 78 to 84 K.
41. We acknowledge helpful discussions with D. R. Nelson and F. Spaepen. This work was supported in part by the Materials Research Science and Engineering Center Program of the National Science Foundation (grant DMR 9400396) and the Office of Naval Research (grant N00014-94-1-0302).

7 May 1996; accepted 17 July 1996

Methane Hydrate and Free Gas on the Blake Ridge from Vertical Seismic Profiling

W. Steven Holbrook, Hartley Hoskins, Warren T. Wood,
Ralph A. Stephen, Daniel Lizarralde,
Leg 164 Science Party

Seismic velocities measured in three drill holes through a gas hydrate deposit on the Blake Ridge, offshore South Carolina, indicate that substantial free gas exists to at least 250 meters beneath the bottom-simulating reflection (BSR). Both methane hydrate and free gas exist even where a clear BSR is absent. The low reflectance, or blanking, above the BSR is caused by lithologic homogeneity of the sediments rather than by hydrate cementation. The average methane hydrate saturation above the BSR is relatively low (5 to 7 percent of porosity), which suggests that earlier global estimates of methane in hydrates may be too high by as much as a factor of 3.

Marine sediments can contain large quantities of natural gas (usually methane) in the form of gas hydrate, a solid compound binding water and gas molecules, which is stable at the high pressures and low temperatures found near the sea floor on continental margins (*1*, *2*). Gas hydrate deposits are identified principally on the basis of their acoustic expression: The phase boundary between methane hydrate and methane plus water gives rise to a prominent negative-polarity event known as a BSR (*3*, *4*), and the addition of hydrate to pore fluids has been interpreted to cause acoustic blanking, a suppression of sediment reflectivity (*5*, *6*). Knowledge of the amount and distribution of methane present as hydrates or free gas is crucial to understanding the potential of methane hydrates as an energy

---

W. S. Holbrook, H. Hoskins, R. A. Stephen, Department of Geology and Geophysics, Woods Hole Oceanographic Institution, Woods Hole, MA 02543, USA.

W. T. Wood, Naval Research Laboratory, Stennis Space Center, MS 39529, USA.

D. Lizarralde, Massachusetts Institute of Technology–Woods Hole Joint Program, Woods Hole Oceanographic Institution, Woods Hole, MA 02543, USA.

resource and their role in the global carbon cycle, continental slope stability, glaciation, and climate change (*2*, *7*–*9*).

Over the past few years, a debate over the precise cause of the BSR (*10*, *11*) has given way to an emerging consensus that the reflection is due principally to free methane gas trapped beneath the hydrate stability zone rather than to the presence of concentrated hydrate just above the phase boundary (*12*–*17*). However, in situ data relating seismic properties to the chemical and sedimentological characteristics of the host sediments and their pore fluids are rare. Knowledge of such fundamental properties as seismic velocity in the hydrate stability zone, the amount of hydrate present in pore spaces above the BSR, and the distribution of free gas beneath the BSR has been lacking, incomplete, or equivocal.

Here, we present the results of vertical seismic profiles (VSPs) acquired on Ocean Drilling Program (ODP) Leg 164 on the Blake Ridge (*18*, *19*), offshore South Carolina (Fig. 1), in an area of prominent acoustic blanking and strong lateral changes in BSR amplitude. A strong BSR occurs at Sites 995 and 997 but disappears at Site 994 (Fig. 2). Zero-offset VSP data were acquired in all three holes (*20*). We analyzed traveltimes of the down-going wave with a constrained least squares inversion (*21*) to yield an accurate measure (within ±50 m/s) of compressional (*P*) wave velocity versus depth (Fig. 2).

In the upper 450 m at all three sites, velocity increases with depth, from ~1550 m/s at 150 m below the sea floor (mbsf) to 1750 to 1850 m/s at 450 mbsf (Fig. 2). This increase primarily reflects a decrease in porosity from about 65 to 50% with depth in the holes. These velocities are broadly consistent with velocity estimates based on ocean-bottom hydrophone data in the area (*14*, *22*) and cast some doubt on substantially lower velocity estimates of 2300 to 2500 m/s elsewhere on the Blake Ridge (*23*). The velocities above the BSR are not unusually high for sediments at these depths and porosities, and, as discussed below, they limit methane hydrate to a small percentage of porosity.

Seismic velocities in the deeper parts of the holes vary significantly for the three sites. At Sites 995 and 997, a decrease in velocity near 440 mbsf indicates that free gas is present beneath the BSR. Site 994, in contrast, lacks a BSR at the expected depth, and velocities do not decrease there until ~550 mbsf. Low seismic velocities (~1500 m/s) in the deeper portions of the holes strongly indicate the presence of free gas in the pore fluid. The free gas zone is surprisingly thick. At Site 997, low velocities persist to the base of the hole, 250 m beneath the BSR. The presence of a thick free gas zone suggests that methane gas is produced well beneath the base of the hydrate stability zone (*24*). A thick free gas zone may not be restricted to rifted margins: VSP and sonic log measurements on the Cascadia accretionary prism (Site 892) show that free gas exists at least 50 m beneath the BSR (*13*).

A comparison of VSP-derived *P* velocities with chemical and lithological data derived from Leg 164 sediment cores shows that reflectance on the Blake Ridge can be explained entirely by two properties: lithologic variations and low velocities indicative of free gas. Strong vertical lithological variations, as evidenced by the total calcium carbonate ($CaCO_3$) content of the sediment, occur in the upper 150 mbsf (Fig. 3, A to C) and are responsible for the shallow reflections observed there (*25*). Deeper (>440 mbsf) reflections, in contrast, are not associated with lithological changes—the section beneath 150 mbsf is remarkably uniform—but instead correlate with low velocities. At Sites 995 and 997, the BSR marks the top of the thick low-velocity zone, and deeper reflections are found within it. At Site 994, where no BSR is observed at 450 mbsf, strong reflections at 550 to 600 mbsf correspond to the top of the deeper low-velocity zone. *P* velocity decreases strongly in the presence of small quantities of free gas (*26*); thus, the reflectivity seen at and beneath the BSR indicates layers containing trapped gas in pore fluids. The numerous reflections within the low-velocity zone (Fig. 2) indicate that gas is trapped between stratigraphic layers, probably by subtle differences in permeability between lithologically similar units. The BSR, therefore, is not the sole indicator of free gas but simply represents the shallowest level at which gas is present.

The amplitude of the BSR is controlled by local concentrations of methane gas in thin (<20 m) layers and is not directly related to the total amount of free gas present beneath the stability zone at a particular site, nor is it related to the amount of hydrate present above the BSR. On the drilling transect, the BSR is strongest at Site 995 (Fig. 3B), but the total amount of free gas in the 250 m beneath the BSR is greatest beneath Site 997, as evidenced by the low average velocities there (Fig. 2). The presence of hydrate above the BSR can be inferred from the Cl^- content of pore waters squeezed from core samples; values that depart from the background Cl^- trend are due to hydrate dissociation during core recovery (*27*) (Fig. 3). The Cl^- values indicate that hydrate is present at all three sites at about 220 to 450 mbsf and that greater amounts of hydrate (revealed by very low Cl^- values) are present at all three

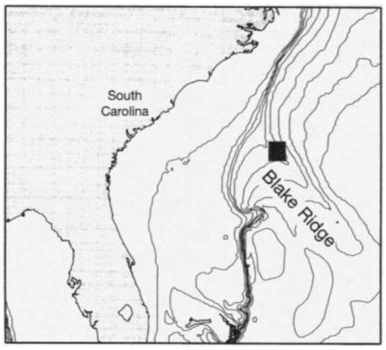

Fig. 1. Location of ODP Leg 164 (box), Blake Ridge. Bathymetric contours are shown at 500-m intervals.

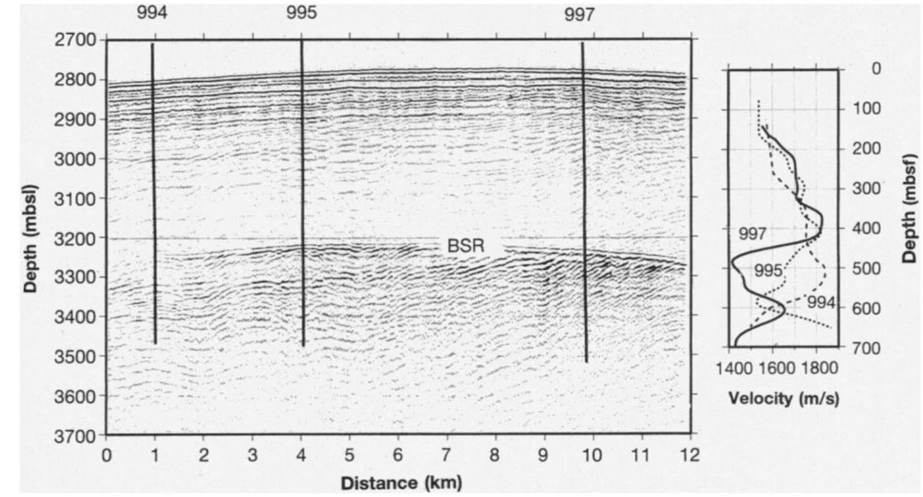

Fig. 2. Single-channel seismic data on Blake Ridge (*14*), depth-converted using velocity-depth functions (right panel) determined from traveltime inversion of vertical seismic profile data. Solid lines show positions of drill holes 994D, 995B, and 997B. Two highly reflective zones are observed: one at 0 to 150 mbsf, and the other at and beneath the BSR [strong reflection at 3220 to 3250 m below sea level (mbsl)].

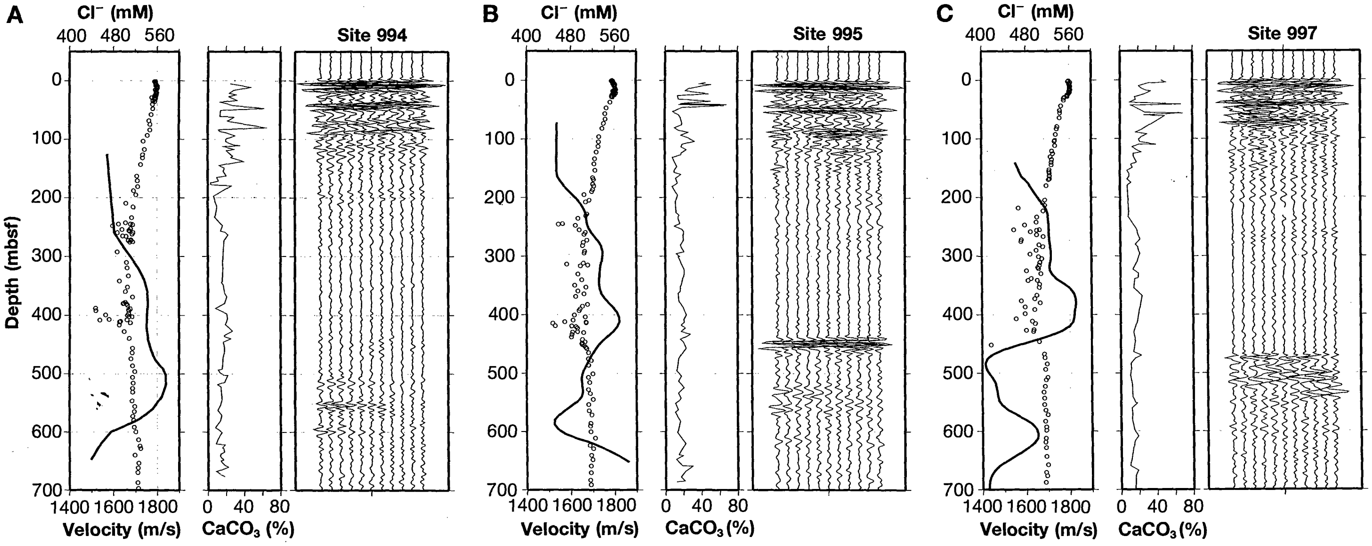

Fig. 3. Comparison of seismic velocity from VSPs, chlorinity ([Cl^-]), $CaCO_3$ content (as weight percent of total matrix), and vertical-incidence seismic reflection data from (**A**) Site 994, (**B**) Site 995, and (**C**) Site 997. Anomalous chlorinity values indicate that methane hydrate is present between 220 and 450 mbsf at all three sites. Seismic reflections correlate with vertical lithological changes in the upper 150 mbsf and with low seismic velocities indicative of free gas (bright spots) beneath the hydrate stability zone. The low reflectance above the BSR is the expected response of lithologically uniform sediments.

sites near the base of the hydrate stability zone (Fig. 3) (*18*, *19*). Yet no BSR is observed at Site 994, which indicates that hydrate can be present even where a BSR is absent.

The low reflectance above the BSR is readily explained as the naturally low background reflectance of a uniform sedimentary section. Sediments drilled on the Blake Ridge consist almost entirely of greenish-gray nannofossil clay (*18*), with little lithologic variation below the uppermost 150 m (Fig. 3). The blanking for which the Blake Ridge is known (*4*–*6*) can thus be attributed to the relative homogeneity of the sediments rather than to hydrate cementation or to diagenesis beneath the BSR (*10*). The reflectance pattern on the Blake Ridge represents not a blanked (cemented) zone overlying strong background reflectance but rather weak background reflectance overlying bright spots, reflections enhanced by gas-charged layers. This finding circumvents two long-standing problems with the blanking hypothesis. First, blanking is not associated with BSRs on convergent margins (*17*, *28*) and is not always observed on rifted margins [for example, the nearby Carolina Rise (*22*)]. Second, any physical model of hydrate cementation that pervasively suppresses impedance contrasts would also raise average *P* velocities well above the modest values (1700 to 1800 m/s) seen in the Blake Ridge section (*29*).

The seismic velocities measured by the VSPs provide a means of estimating the mass of methane present as hydrate and free gas on the Blake Ridge. Velocities from 200 to 450 mbsf are consistent with hydrate filling 2% of porosity at Site 994 and 5 to 7% of porosity at Sites 995 and 997 (*30*). A 200-m-thick zone with 55% porosity containing 5% hydrate produces a 5-m "equivalent thickness" of pure hydrate in the sediment column, substantially less than prior estimates of >30 m for this part of the Blake Ridge based on a model of acoustic blanking (*5*). A 5-m thickness of hydrate in the sediment column yields 615 kg of methane per square meter of area (*31*). If we assume that half of this hydrate concentration is representative of the ~100,000 km^2 area interpreted to contain methane hydrates on the southeast U.S. margin (*5*), then a total of ~30 billion metric tons (Gt) of methane (~23 Gt of carbon) exists as hydrate there.

Although our estimate of the amount of methane hydrate is lower than earlier estimates, the considerable thickness of the free gas zone implies that far more methane is present beneath the BSR than previously realized. The velocity decrease to 1500 to 1600 m/s at all three sites yields a conservative estimate of 1% of porosity, on average, occupied by free gas. This yields 1 kg of methane per cubic meter of sediment (*32*). If the free gas zone is 200 m thick beneath the BSR (as appears to be the case at Site 995 and is a minimum estimate for Site 997), then free gas adds ~200 kg of methane per square meter of area, adding to the inventory of methane from hydrate beneath the Blake Ridge by nearly one-third. If only half of this amount of free gas is representative of the hydrate-bearing region of the southeastern U.S. Atlantic margin, then 10 Gt of methane (7.5 Gt of carbon) is present in gas bubbles. The total amount of methane in hydrate and free gas may therefore be ~40 Gt.

Most previous estimates of hydrate saturation on other (mostly convergent) margins exceed our estimate of 5 to 7% of porosity (*33*, *34*). Kvenvolden and Grantz (*34*) calculated 540 Gt of carbon as methane in sediment on the Arctic margin off Alaska, 18 times our estimate in an area only five times as large. Our results suggest either that the Blake Ridge contains less methane per unit area than other continental margins where hydrates have been studied (which is possible but seems unlikely, given the thick free-gas zone at the Blake Ridge) or that global estimates of methane in hydrates (*9*, *35*) are too high by as much as a factor of 3.

REFERENCES AND NOTES

1. G. E. Claypool and I. R. Kaplan, in *Natural Gases in Marine Sediments*, I. R. Kaplan, Ed. (Plenum, New York, 1974), pp. 99–139; E. D. Sloan, *Clathrate Hydrates of Natural Gases* (Decker, New York, 1989); K. A. Kvenvolden and L. A. Barnard, *Am. Assoc. Pet. Geol. Mem.* **34**, 634 (1982).
2. K. A. Kvenvolden, *Global Biogeochem. Cycles* **2**, 221 (1988).
3. R. G. Markl, G. M. Bryan, J. I. Ewing, *J. Geophys. Res.* **75**, 4539 (1970); J. I. Ewing and C. D. Hollister, *Init. Rep. Deep Sea Drill. Proj.* **11**, 951 (1972); B. E. Tucholke, G. M. Bryan, J. I. Ewing, *Am. Assoc. Pet. Geol. Bull.* **61**, 698 (1977).
4. T. H. Shipley *et al.*, *Am. Assoc. Pet. Geol. Bull.* **63**, 2204 (1979).
5. W. P. Dillon, M. W. Lee, K. Fehlhaber, D. F. Coleman, *U.S. Geol. Surv. Prof. Pap. 1570* (1993), pp. 313–330.
6. M. W. Lee *et al.*, *Mar. Geophys. Res.* **16**, 163 (1994).
7. C. K. Paull, W. Ussler III, W. P. Dillon, *Geophys. Res. Lett.* **18**, 432 (1991).
8. B. U. Haq, *Spec. Publ. Int. Assoc. Sedimentol.* **18**, 93 (1993).
9. K. Kvenvolden, *Chem. Geol.* **71**, 41 (1988).
10. R. D. Hyndman and E. E. Davis, *J. Geophys. Res.* **97**, 7025 (1992).
11. R. D. Hyndman and G. D. Spence, *ibid.*, p. 6683.
12. N. L. Bangs, D. S. Sawyer, X. Golovchenko, *Geology*

21, 905 (1993).
13. M. E. MacKay, R. D. Jarrad, G. K. Westbrook, R. D. Hyndman, Shipboard Scientific Party of ODP Leg 146, *ibid.* **22**, 459 (1994).
14. R. Katzman, W. S. Holbrook, C. K. Paull, *J. Geophys. Res.* **99**, 17975 (1994).
15. T. A. Minshull, S. C. Singh, G. K. Westbrook, *ibid.*, p. 4715.
16. S. C. Singh, T. A. Minshull, G. D. Spence, *Science* **260**, 204 (1993).
17. S. C. Singh and T. A. Minshull, *J. Geophys. Res.* **99**, 24221 (1994).
18. R. Matsumoto, C. Paull, P. Wallace, *Init. Rep. Deep Sea Drill. Proj.*, in press.
19. ODP Leg 164 Shipboard Science Party, *Eos* **77**, 219 (1996).
20. We acquired VSP data by firing a 300-cubic-inch (4.9-liter) air gun and recording the shots on a three-component Woods Hole Oceanographic Institution borehole seismometer clamped at 8-m intervals from about 150 to 700 mbsf. Ten to 20 air-gun shots were recorded at each depth and summed to form a stacked section.
21. We perform a weighted, damped, least squares inversion of VSP traveltimes for slowness, minimizing $L = \|T - ZU\| + \mathscr{E}\|P\|$, where T, Z, and U are, respectively, the traveltime, depth, and slowness vectors, P is the second derivative of U, and $\mathscr{E}$ is the Lagrange parameter that governs trade-off between data misfit and model smoothness. We chose $\mathscr{E}$ to be 2.5 to 3.0 for the inversions shown here. The traveltime data cannot resolve thin (<20 m thick) high- or low-velocity layers.
22. J. Korenaga, W. S. Holbrook, S. C. Singh, T. A. Minshull, *J. Geophys. Res.*, in press.
23. M. M. Rowe and J. F. Gettrust, *ibid.* **98**, 463 (1993).
24. Free gas may be produced by several processes: (i) breakdown of hydrate at the BSR as sediment passes downward out of the hydrate stability zone; (ii) in situ biogenic or thermogenic methanogenesis; or (iii) distillation of gas if pore fluid saturated in dissolved methane moves either upward or downward into a region of lower solubility [C. K. Paull, W. Ussler III, W. Borowski, *Ann. N.Y. Acad. Sci.* **715**, 392 (1994)].
25. L. A. Mayer, *Nature* **352**, 148 (1991).
26. S. N. Domenico, *Geophysics* **42**, 1339 (1977); M. N. Toksöz, C. H. Cheng, A. Timur, *ibid.* **41**, 621 (1976).
27. R. Hesse and W. E. Harrison, *Earth Planet. Sci. Lett.* **55**, 453 (1981).
28. J. J. Miller, M. Y. Lee, R. von Huene, *Am. Assoc. Pet. Geol. Bull.* **75**, 910 (1991).
29. M. W. Lee *et al.*, *Mar. Pet. Geol.* **10**, 493 (1993).
30. A weighted mean of the Wood and Wyllie equations [equation 4 of (*29*)] expresses seismic velocity as a function of matrix velocity, porosity, and hydrate content. We used a matrix velocity of 4.37 km/s, water velocity of 1.5 km/s, hydrate velocity of 3.3 km/s, matrix density of 2700 kg/m^3, water density of 1000 kg/m^3, hydrate density of 900 kg/m^3, a weighting factor of 1.0, and porosity values calculated on shipboard samples (*18*). For example, at a depth of 250 mbsf, the shipboard-measured porosity of 60% implies 5% saturation of hydrate to yield a velocity of 1700 m/s.
31. The density of methane in methane hydrate is 123 kg/m^3, calculated from the gram molecular weight of 16 g/mol for methane and 7700 mol/m^3 of hydrate [M. A. Mathews and R. von Huene, *Init. Rep. Deep Sea Drill. Proj.* **84**, 773 (1985)].
32. This value is based on 50% porosity and a density of methane of 200 kg/m^3 at 3200 m below sea level, calculated on the assumption of ideal gas behavior.
33. G. D. Spence, T. A. Minshull, C. Fink, in *Proceedings of the Ocean Drilling Program, Scientific Results (Pt. I)*, B. Carson, G. K. Westbrook, R. J. Musgrave, E. Suess, Eds. (Ocean Drilling Program, College Station, TX, 1995), vol. 146, pp. 163–174.
34. K. A. Kvenvolden and A. Grantz, in *The Arctic Ocean Region*, A. Grantz, L. Johnson, J. F. Sweeney, Eds. (Geological Society of America, Boulder, CO, 1990), pp. 539–549.
35. K. A. Kvenvolden, *Rev. Geophys.* **31**, 173 (1993).

36. We thank the crew of the *Joint Oceanographic Institutions for Deep Earth Sampling Resolution* for their untiring efforts during the drilling and VSP work, especially A. Ribbens, S. Kittredge, K. Kuroki, R. Current, B. Julson, N. Smith, R. Johnson, G. Pollard, and R. Caldow. For enlightening discussions during this work we thank W. Dillon, D. Hutchinson, J. Booth, J. Korenaga, and I. Pecher. Technical assistance ashore was provided by K. Peal, T. Bolmer, R. Busby, S. Rosenblad, M. Gould, and D. Dwyer. We thank the Incorporated Research Institutions for Seismology–Program for Array Seismic Studies of the Continental Lithosphere center at Lamont-Doherty Earth Observatory for loan of Reftek data loggers and software. Supported by JOI-USSAC subaward 7-95 and NSF grant OCE-9504610.

17 May 1996; accepted 12 August 1996

Peculiarities of Methane Clathrate Hydrate Formation and Solid-State Deformation, Including Possible Superheating of Water Ice

Laura A. Stern,* Stephen H. Kirby, William B. Durham

Slow, constant-volume heating of water ice plus methane gas mixtures forms methane clathrate hydrate by a progressive reaction that occurs at the nascent ice/liquid water interface. As this reaction proceeds, the rate of melting of metastable water ice may be suppressed to allow short-lived superheating of ice to at least 276 kelvin. Plastic flow properties measured on clathrate test specimens are significantly different from those of water ice; under nonhydrostatic stress, methane clathrate undergoes extensive strain hardening and a process of solid-state disproportionation or exsolution at conditions well within its conventional hydrostatic stability field.

Gas hydrates, also called clathrate hydrates, are nonstoichiometric compounds with structures consisting of a network of H_2O molecules hydrogen-bonded together like ice and encaging molecules of small-diameter gases. Common natural gas hydrates may have either of two crystal structures, and methane hydrate, $CH_4{\cdot}5.75H_2O$ (ideally), is a structure I hydrate constructed from 46 H_2O molecules with eight cavities available for CH_4 gas molecules. In addition to its possible occurrence on the icy moons of the outer solar system at Saturn and beyond (*1*), methane clathrate occurs on Earth in a variety of geologic settings where CH_4 and H_2O are in chemical contact at low temperature (T) and elevated pressure (P), and possibly harbors the largest untapped reservoir of natural gas on Earth (*2*, *3*). Although discovery of extensive clathrate reservoirs in sediments underlying permafrost regions, deep-oceanic environments, and continental margins and shelves has stimulated recent interest in their formation and recoverability (*4*), many basic physical properties of methane clathrate are poorly known or unmeasured. We have developed a method for fabricating pure aggregates of methane clathrate in quantities suitable for materials testing and have documented anomalous behavior in the formation, stability, and rheology of this compound at elevated P (*5*).

Our objective was to synthesize large-volume, low-porosity, cohesive polycrystalline clathrate aggregates with a uniform fine grain size and random crystallographic grain orientation. Our technique differed from those of previous studies (*6*), most of which involved dynamic conditions of rocking, rotation, or continuous agitation of reaction mixtures, resulting in loose or very porous granular aggregates or strongly textured material unsuitable for physical property measurements. We produced our samples by the reaction CH_4 (g) + $6H_2O$ (s $\rightarrow$ l) $\rightarrow$ $CH_4{\cdot}6H_2O$ (s), by the mixing and subsequent slow, regulated heating of sieved, granular H_2O ice and cold, pressurized CH_4 gas in an approximately constant-volume

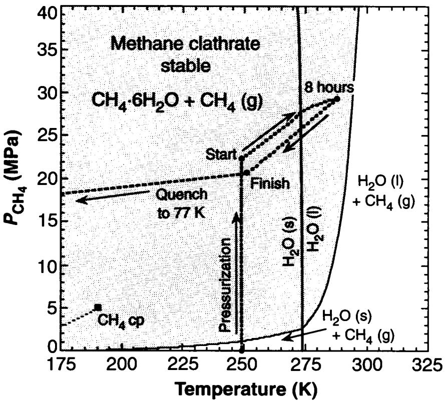

Fig. 1. Phase diagram for the CH_4-H_2O system. Shaded region shows field of methane clathrate stability. At low pressures or high temperatures, clathrate dissociates to H_2O plus CH_4 gas. The metastable extension of the H_2O melting curve is delineated by the gray curve. Dotted lines trace the sample fabrication reaction path.

L. A. Stern and S. H. Kirby, U.S. Geological Survey, Menlo Park, CA 94025, USA.
W. B. Durham, Lawrence Livermore National Laboratory, Livermore, CA 94550, USA.

*To whom correspondence should be addressed.